Journal of Solid State Chemistry 184 (2011) 3055–3061

Contents lists available at SciVerse ScienceDirect

Journal of Solid State Chemistry

journal homepage: www.elsevier.com/locate/jssc

Scalable synthesis and characterization of cobalt sodium tartrate nanowires with adjustable diameters

Lan Chen, Shaochun Tang, Sascha Vongehr, Kun Hu, Xiangkang Meng *

National Laboratory of Solid State Microstructures, Department of Materials Science and Engineering, Nanjing University, Nanjing 210093, PR China

ARTICLE INFO

Article history:
Received 13 May 2011
Received in revised form
2 September 2011
Accepted 11 September 2011
Available online 21 September 2011

Keywords:
Nanowires
Metal organic materials
Hydrothermal synthesis

ABSTRACT

Cobalt sodium tartrate nanowires are synthesized by a simple hydrothermal method using ethanol–water mixed solvents. The smooth wires are on average 30 μm long. Their diameters are narrowly size distributed with a controllable average in the range from 80 to 250 nm. Interestingly, after the initial two hours, the diameter decreases with further reaction time. The tartrate anions act as coordination ligands with all six oxygen atoms participating in the coordination. The Co^{2+} and Na^{+} ions chelate with the O atoms from the carboxylate and hydroxyl groups in the tartrate ligands. The ethanol participates in the formation of pi bonds. The cobalt is divalent while the sodium is monovalent in their tartrates. The respective crystal structures of these metal tartrates are incompatible, and the wires are therefore amorphous. The influence of the reaction time, sodium tartrate concentration, pH value, and the ethanol water ratio are studied in detail.

© 2011 Elsevier Inc. All rights reserved.

1. Introduction

Materials composed of metal ions and organic ligands have been of immense recent research interest [1–6]. Such metal-organics are the basis of new solid functional materials with broad applications in areas such as catalysis [7], gas storage [8], magnetism [4,9], semiconductors [10], and optics [11]. Since the properties of nanometer sized components are highly shape-dependent, much work has been devoted to the shape-controlled synthesis of metal organic nanostructures (NSs) and diverse shapes have been achieved [11–15]. One-dimensional (1D) NSs are especially promising for the manufacture of advanced functional materials. Architectures such as rings [1], chains [7,11], and ladders [11–13] have been prepared and investigated extensively also in order to understand growth phenomena. Properties of 1D nanomaterials are size-dependent [16,17], therefore it is vital to synthesize narrowly selected sizes for applications and research. The majority of the reported 1D metal organics is composed of ligands with large molecular groups. The comparably small hydroxyl polycarboxylates such as malate, citrate, and tartrate have been less studied, although they display versatile coordination modes [3,4,8].

Among the available methods, hydrothermal synthesis has been extensively used for the preparation of various metal organic materials [18–23]. It provides a general route to control size, morphology, microstructures, and phase composition of the products via adjusting reaction parameters such as temperature, process duration, and pH value [19–22]. Especially the choice of solvent plays an important role in the shape control of metal organics [20,22]. Hydrothermal synthesis is a simple, low cost method that is scalable to industrial levels. However, there remains a challenge to synthesize size-adjustable nanowires hydrothermally without surfactant additives [21,23].

In this work, we report the synthesis of long cobalt sodium tartrate nanowires (CSTNWs) using an environmentally friendly, ethanol-assisted hydrothermal procedure without the need of surfactants. The dry products as well as their ethanol dispersions are stable. The diameters of the CSTNWs can be narrowly controlled inside of a wide range. The products were characterized by scanning and transmission electron microscopy and various other spectroscopic techniques. The influence of four reaction parameters on the formation of the wires was investigated: the reaction time, sodium tartrate concentration, pH value, and the ethanol to water ratio. The average diameter can be adjusted via the reaction time and surprisingly shrinks with longer times in most of the investigated regime. A possible growth mechanism of the CSTNWs is proposed.

2. Experimental section

2.1. Synthesis

All chemicals were purchased from Sinopharm Chemical Reagent Co. Ltd. The chemicals are of analytical grade and used

* Corresponding author. Fax: +86 25 8359 5535.
E-mail address: mengxk@nju.edu.cn (X. Meng).

0022-4596/$ - see front matter © 2011 Elsevier Inc. All rights reserved.
doi:10.1016/j.jssc.2011.09.009

as-received without further purification. Deionized water with a resistivity above 18.0 MΩ cm was used directly from a JL-RO100 Millipore-Q Plus water purifier. In a typical procedure, 356.9 mg cobalt chloride ($CoCl_2 \cdot 6H_2O$), 5.177 g sodium L-tartrate ($Na_2C_4H_4O_6 \cdot 2H_2O$), and 3 g sodium hydroxide (NaOH) were dissolved in a 50 °C ethanol–water mixed solvent (33 ml ethanol and 66 ml deionized water) in this stated succession one after another. The ratio r will always denote the volume of ethanol divided by the volume of water before mixing, i.e. $r=1:2$ in the typical experiment. After homogeneous stirring, the resulting transparent, dark green solution was transferred into an 88 ml poly(tetrafluoroethylene) (PTFE, Teflon) lined stainless steel autoclave to fill its volume half. Subsequently, the autoclave was sealed, and maintained at 120 °C for 16 h, then allowed to cool to room temperature. Mauve fluffy solids deposited on the bottom of the Teflon cup. The precipitate was collected, washed with deionized water and ethanol by several centrifuging/re-dispersion cycles, and dried in a vacuum oven for 8 h at 40 °C. Finally a fleece like product was obtained.

2.2. Characterizations

The size, morphology, and composition of the products were characterized by scanning electron microscopy (SEM) and energy dispersion spectroscopy (EDS) on a XL30 ESEM FEG scanning electron microscope at an accelerating voltage of 15 kV. EDS measurements were performed under a low resolution SEM mode and repeated several times in order to get accurate composition information. Transmission electron microscopy (TEM) images and the corresponding selected area electron diffraction (SAED) patterns were taken on an FEI TECNAI F20 microscope operating at 200 kV acceleration. TEM samples were prepared by dispersing the products in alcohol, dropping the suspension onto a carbon film supported on a copper grid, and drying in air. X-ray diffraction (XRD) measurements were carried out on a SHIMADZU XRD-6000 instrument employing Cu $K\alpha$ radiation ($\lambda=0.154$ 187 nm). X-ray photoelectron spectroscopy (XPS) was performed on a Thermo ESCALAB 250 system with a monochromatic Al $K\alpha$ X-ray source ($h\nu=1486.6$ eV, 150 W). All the binding energies were referenced to the C 1s peak at 284.8 eV as internal standard. The Fourier transform infrared (FT-IR) spectrum was recorded with a NEXUS870 spectrometer in the range of 400–4000 cm^{-1} using a KBr wafer. Thermogravimetry–differential scanning calorimetry (TG–DSC) was performed on a NETZSCH-STA 409 PC simultaneous thermal analyzer (NETZSCH, Germany) with a heating rate of 5 °C/min from ambient temperature to 800 °C in flowing N_2 atmosphere.

3. Results and discussion

3.1. Microscopy and X-ray diffraction

Fig. 1a shows a digital camera photograph of the product dispersed in alcohol. The suspension exhibits a fleece like product with pink color. A low-magnification SEM image (Fig. 1b) reveals that the product consists only of nanowires. The length of the wires reaches up to 30 μm. A magnified SEM image (Fig. 1c) indicates that they have smooth surfaces and a narrow size distribution with an average diameter of (80 ± 20) nm. Note that what looks like very thick wires are actually aligned pairs (see white arrow, also very clear in Fig. 1e). In order to investigate the shape of the cross sections of the wires, the following method has been employed: the samples were prepared by dispersing the products in alcohol and dropping the suspension onto a Pt/Si substrate that was previously scribed with a diamond knife. After drying in air, the substrate was broken along the scratch and fastened on the microscope stage exposing the broken edge. Many end sections of wires are thus seen. As shown in Fig. 1d, the cross sections of the wires are circular (see white arrows). If they were

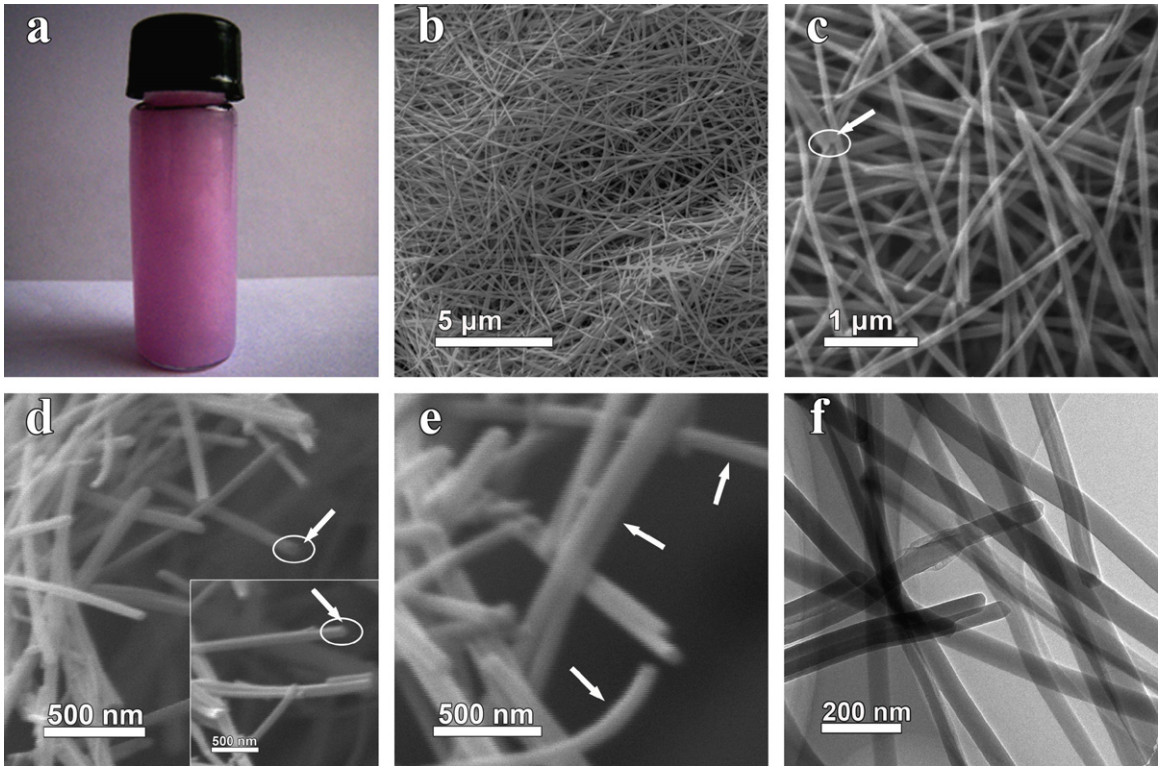

Fig. 1. A digital photo showing the suspension of the product (a), SEM images with different magnifications (b and c), SEM images showing wire cross sections (d and e), and a TEM image (f) of typical products.

belts or had an elliptical cross section instead, the visible ellipses would be narrower and at different, random angles. The bend wires for example visible in Fig. 1e (white arrows) further confirm the circular cross sections. When belts bend, they naturally bend with the curvature radius normal to the flat side of the belt, which would result in images having projections with changing diameters along the length of such belts. The diameters along our product's bend wires' SEM images are constant, indicating circular cross sections everywhere. Fig. 1f shows a bright-field TEM image, which confirms the narrow distribution of diameters around 80 nm. The ends of the wires are smooth and round (Fig. S1). No crystal lattice is observed in high resolution TEM (HRTEM) images (Fig. S1b). The corresponding SAED pattern recorded from an individual nanowire (inset in Fig. S1b) also demonstrates the amorphous nature. The XRD pattern (Fig. S2) presents a very broad peak characteristic of amorphous structure. Crystalline nanowires are usually the result of growth along a certain crystallographic direction [16,17]. To our knowledge, non-crystalline metal organic nanowires with high uniformity in diameters have not been reported. The products appear unchanged after being kept in ethanol for several months.

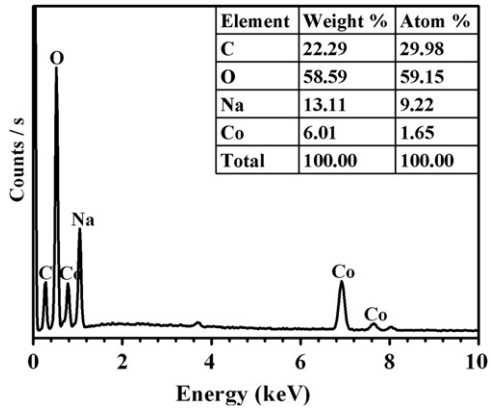

Fig. 2. EDS pattern recorded from the nanowires shown in Fig. 1. The inset tabulates the elemental composition assignments.

3.2. Composition and structure analysis

Fig. 2 presents a typical EDS pattern recorded from the same sample as shown in Fig. 1. Besides the Cu signals from the SEM copper substrate, only C, O, Co and Na are detected and no impurities are found. The atomic percentages (atom %) of C, O, Na, and Co in the product are 29.98, 59.15, 9.22 and 1.65, respectively (inset in Fig. 2).

XPS measurements were used to investigate the chemical states of the elements and structure of the nanowires. Fig. 3a shows the XPS survey spectrum of the sample shown in Fig. 1. Based on peaks due to the binding energies, the elements in the compound are established. They are at 285 eV for C 1*s*, 531 eV for O 1*s*, 782 eV for Co 2*p* and 1073 eV for Na 1*s* [24]. The spectrum of the Co 2*p* scan (Fig. 3b) presents a Co $2p_{3/2}$ binding-energy peak at 781.4 eV and a Co $2p_{1/2}$ peak at 797.5 eV, revealing that the Co in the sample is purely bivalent [24,25]. This may be due to the formation of the complex ions of $Co(C_4H_2O_6)^{2-}$ as intermediates during the reaction. The ion complex avoids the generation of cobalt hydroxide and the further oxidization of cobalt [26]. The O 1*s* spectrum consists of two peaks, one at 531.6 eV due to C=O and C–OH, and one at 535.9 eV due to H_2O (Fig. 3c) [24,27,28]. In the C 1*s* spectrum (Fig. 3d), peak A at 288.58 eV and peak B at

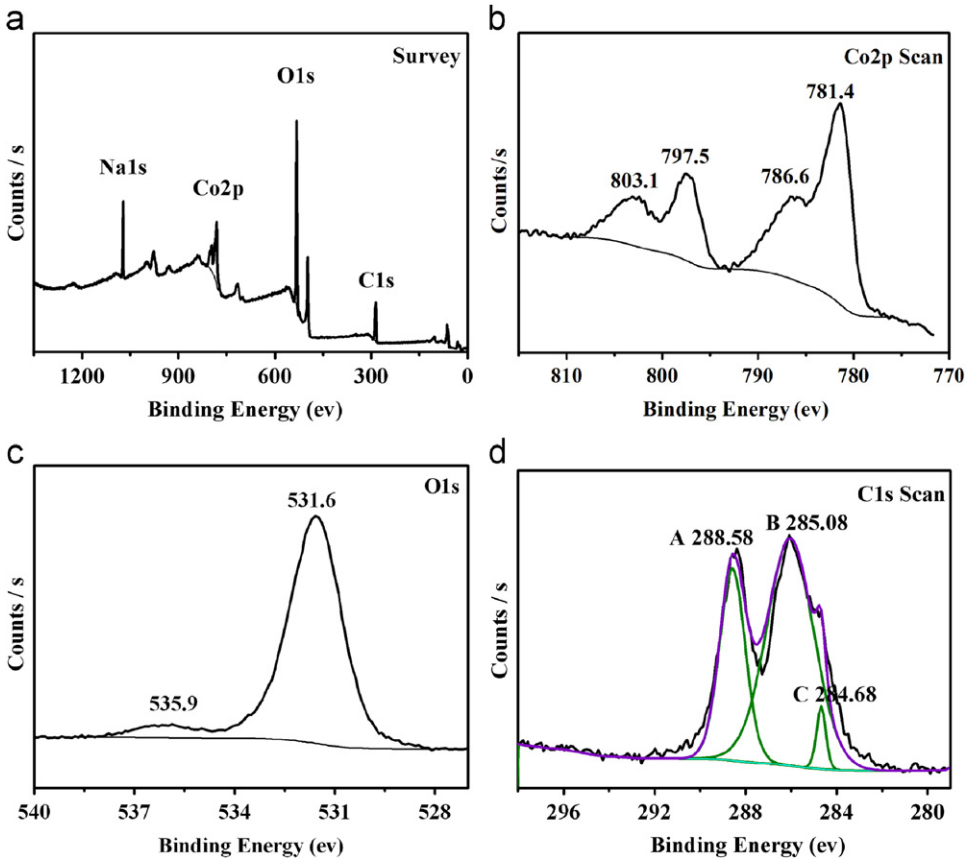

Fig. 3. XPS spectra: survey (a), Co 2*p* (b), O 1*s* (c), and C 1*s* (d) scans of the sample shown in Fig. 1.

285.08 eV are both in a range compatible with tartrate anions, while peak C at 284.68 eV and also peak B are indicative of ethanol [24,27]. It implies that both, tartrate anion and ethanol are contained in the product. The molar ratio between tartrate and ethanol is about 7:1 as estimated from the areas under the peaks in the C 1*s* spectrum. This is consistent with the atomic percentages of carbon and oxygen calculated from the survey spectrum. On the basis of the analysis of XPS spectra, it is suggested that apart from the two metals, the product is composed of tartrate anions, ethanol, and water.

FT-IR spectroscopy was performed to reveal the molecular structure of the CSTNWs. A broad band and several narrow peaks are observed in the range of 400–4000 cm^{-1} (Fig. 4). The molecular group vibrations are assigned according to the commonly used reference [29] and the IR spectra of tartrate salts [30,31] (Table 1). The strong and broad band at 3427 cm^{-1} is due to the ν(OH) stretching vibrations of water and COOH groups [29,30]. A weak peak at 2854 cm^{-1} is assigned to C–H symmetric stretching. Three strong peaks at 1579, 1397, and 1128 cm^{-1} are attributed to: ν_{as}(C=O) asymmetric stretching of the carbonyl groups (1), ν_s(C=O) symmetric stretching and δ(O–C=O) deformation vibration modes (2), and δ(C–H) deformation vibration as well as π(C–H) skeletal vibration modes (3), respectively. The weak peak next to the 1397 cm^{-1} peak is also due to ν_s(C=O) symmetric stretching, and the small separation between these two peaks is a characteristic of tartrate salts [29–31]. The two peaks are shifted to lower frequencies compared to free tartrate acid, which suggests the existence of interactions between the metals and tartrate ligands. This linkage between the metal atoms and the carboxylate groups is confirmed by both the broadening and a distinct shift of the ν_{as}(C=O) asymmetric stretching band. It shifts from 1743 cm^{-1} in the free tartaric acid to 1579 cm^{-1} due to a reduction of bond order in complexation [31]. The peaks at 923, 846, and 808 cm^{-1} are attributed to various types of C–OH out of plane bending vibration modes. The sharp peak at 729 cm^{-1} results from C–C=O in plane bending vibration modes. The band ranging from 450 to 620 cm^{-1} is assigned to metal–oxygen bonds and C–C=O out of plane bending modes [29–31]. The FT-IR spectroscopy confirms that the product is composed of tartrate anions, ethanol, and water. It is suggested that ethanol participates in the formation of pi bonds, while water molecules bind to the product by hydrogen and Van der Waals bonds [30,31].

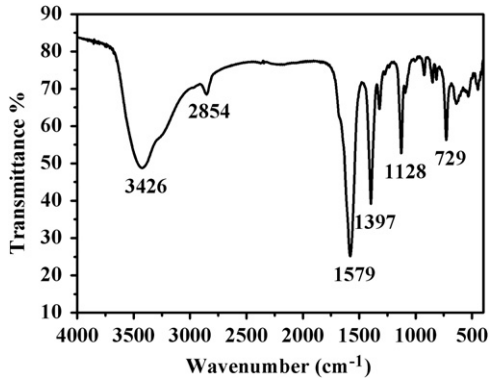

Fig. 4. FT-IR spectrum of the CSTNWs recorded in the range of 400–4000 cm^{-1}.

Table 1
Assignment of some selected FT-IR wave numbers.

Wave number/cm^{-1}	Assignments
3427	ν(−OH) stretch influenced by water and ethanol
2854	ν_s(C–H) sym stretch
1579	ν_{as}(C=O) stretch of the carbonyl group
1397	ν_s(C=O) and δ(O–C=O) modes
1322	ν_s(C=O) mode
1128	δ(C–H)+π(C–H) C–H skeletal stretch
923, 846, 808	γ(C–OH) out of plane bend
729	β(C–C=O) in plane bend
450–619	metal–oxygen bonds and γ(C–C=O) out of plane bend

The dry CSTNW powder was analyzed by thermogravimetry–differential scanning calorimetry (TG–DSC) as presented in Fig. S3. The mass loss occurring between 40 and 250 °C in the thermogravimetric analysis (TGA) curve and the two corresponding, weak endothermic peaks at 77.2 and 235.3 °C in the DSC curve imply the existence of both absorbed and bonded water. The strong exothermic peak at 318.7 °C in the DSC curve corresponds to the huge mass loss in the second stage of decomposition between 250 and 340 °C in the TGA curve. It indicates the conversion from tartrates into oxalates. The oxalates decomposed into oxides between 590 and 770 °C. The mass loss in each stage approximately corresponds to the proposed reaction (see Supporting Information), which in turn supports the composition and structure analysis.

3.3. *Effects of reaction parameters*

The diameters of the CSTNWs are time-dependent and can thus be controlled. Fig. 5 shows the wire diameter versus reaction time t while other reaction parameters were kept the same as those for the sample shown in Fig. 1, the parameters of which we will henceforth refer to as "typical". The diameters of the nanowires prepared in a short reaction time of only 1 h have a large value of (200 ± 60) nm (Fig. 5a). Their lengths reach nearly 30 μm. After 2 h (Fig. 5b), the average diameter of the wires is about 250 nm but the dispersion decreased (±50 nm); their length is about 30 μm. As t is further increased to 4 h (Fig. 5c), the diameters decrease to 110 nm while the dispersion decreases continually (±30 nm). Increasing t to 12 h results in nanowires with yet smaller diameters of (100 ± 30 nm) (Fig. 5d). The length of the wires still reaches up to 30 μm and it has thus, if at all, not changed by the same ratio as the diameter. When t=16 h (Fig. 1), the uniformity of the diameter is yet better (±20 nm) with the average diameter being the smallest at 80 nm. Thus, different diameters of nanowires can be achieved through adjusting t. Since the change is not linear and most of the change occurs at small reaction times, we did not investigate yet longer times. The diameter does only decrease during the hydrothermal treatment but stays stable for months if the product is stored in ethanol.

The concentration c of sodium tartrate influences the product's morphology and composition. In the typical experiment, c is 0.225 M, which results in a saturated solution given the typical solvent ratio of r=1:2 and at 50 °C. At half of this typical concentration, a mixture consisting of wires and coral-like NSs is obtained instead (Fig. 6a and b). When c was decreased further, only the coral-like β-$Co(OH)_2$ NSs were obtained [20]. The fact that low concentration leads to β-$Co(OH)_2$ indicates that close to saturated sodium tartrate is necessary for the exclusive formation of CSTNWs. The changes of composition and morphology of the products should be due to the competition between hydroxyl anions and tartrate anions, which can both coordinate with the metal anions.

The pH value is also important for the formation of the nanowires. A strong alkaline environment of pH > 13.5 is needed for the reaction. A pH of 13.3 already leads to a large dispersion of the diameters and the product will dissolve in water in a few minutes during the washing process, whereas product synthesized at larger pH values will not change in water over several

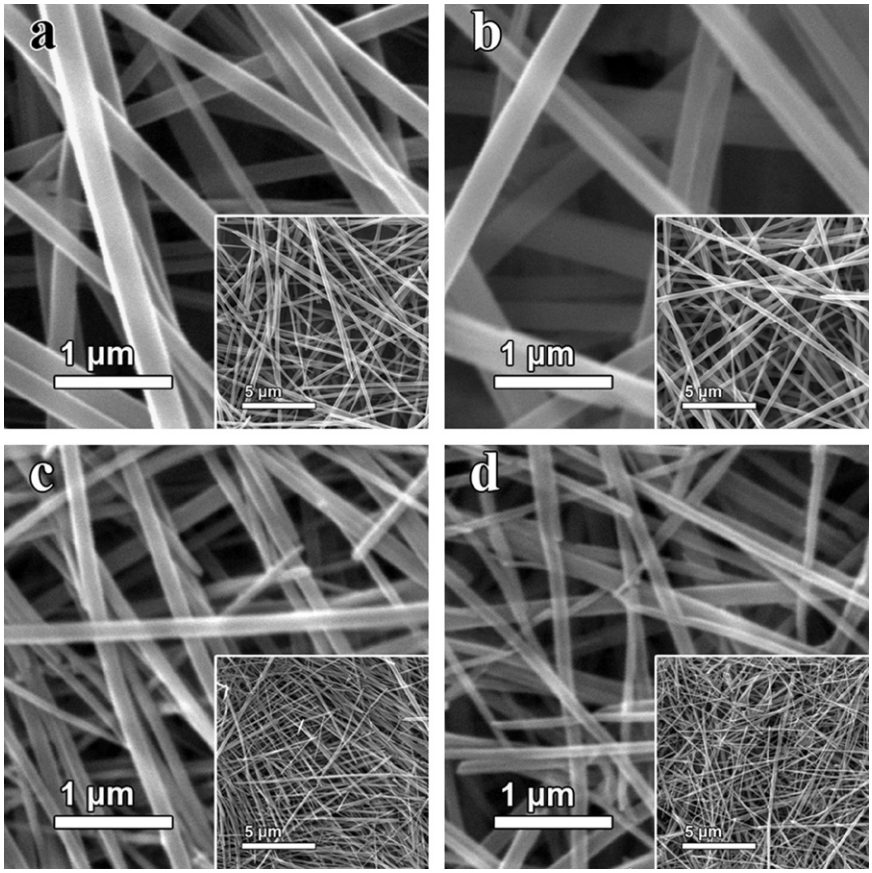

Fig. 5. SEM images of the products obtained with different reaction times of 1 (a), 2 (b), 4 (c), and 12 (d) hours with other conditions kept constant.

days. If the pH value is about 7 (no NaOH), products with irregular shapes are obtained (Fig. S4).

Ethanol has been demonstrated to have strong influence on the morphologies of products in similar hydrothermal syntheses [20]. In this work, ethanol is again a key factor. Without ethanol ($r=0$) while other reaction conditions remained typical, no nanowires but products with irregular shapes were obtained. With an increase of the ethanol ratio r, the products' diameters become less dispersed (Fig. 6c and d) and the diameters decrease. When $r=1{:}4$ (Fig. 6c), the average diameter is (240 ± 135) nm, and some very thick and thin wires exist. With $r=1{:}3$ (Fig. 6d), the average diameter is (220 ± 90) nm, while $r=1{:}2$ (Fig. 1) results in an average diameter of (80 ± 20) nm. A higher than typical ethanol content was not explored because the sodium tartrate cannot dissolve completely in the mixed solvent when r is above 1:2.

On the basis of the experiments with different reaction parameters, suitable conditions for the synthesis of CSTNWs at a hydrothermal temperature of 120 °C are as follows: the optimal concentration of sodium tartrate is $c=0.225$ M, the ethanol ratio should be $r=1{:}2$, and the pH value above 13.5. The reaction time t should be about 5 h, because the largest drop in the dispersion of the diameters happens around $t=4$ h.

3.4. Discussion of structure and growth mechanism

For most divalent metals, their tartrate salts are built from a common structural building block, namely a dimer with the general formula $[M_2(\text{L-tart})_2X_n]^{y-}$ (Fig. 7), in which M is the metal ion, L-tart is the L-tartrate ion, and X is a solvent molecule or another kind of capping ligand [4,32]. As illustrated in Fig. 7b, the metal center A is chelated by two tartrate ligands with one oxygen atom from the carboxylate group and another from an adjacent OH group. The other carboxylate and adjacent OH groups of the tartrate ligands chelate with another metal center B. Thus, each tartrate ligand chelates with two metal centers in the dimer [4,32]. In each building block, the metals bind with the four oxygen atoms provided by two tartrate ions, with oxygen atoms from solvent molecules, and with nonchelating carboxylate oxygen atoms from adjacent dimers, to form an octahedral coordination structure [32]. Since the metal centers chelate with tartrate ions of adjacent units, a regular 3D network is formed based on this octahedral coordination structure. This structure is true also for mixtures of divalent metals, like nickel cobalt tartrate [4].

In the tartrate salts of monovalent metals, e.g. sodium tartrate or sodium potassium tartrate [3], two kinds of metal locations exist and the metals must share O atoms. Their coordination mechanism in the 3D framework is similar to that of divalent metal tartrate salts considering the chelating between metals and tartrate ions of neighboring units [33,34]. However, their crystal structures are different.

The metals in the CSTNWs have different valences, since the cobalt is divalent but the sodium is monovalent, as demonstrated by the XPS spectra in Fig. 3. Therefore, neither the monovalent nor the divalent metal tartrate structure can grow and an amorphous material forms instead. Due to the structure difference between cobalt tartrate and sodium tartrate, potential remaining coordination sites of the metal centers exist. Those sites are occupied by ethanol and water molecules [3,4,34,35].

That the diameters decrease with reaction time while the lengths stay constant is an interesting phenomenon, which

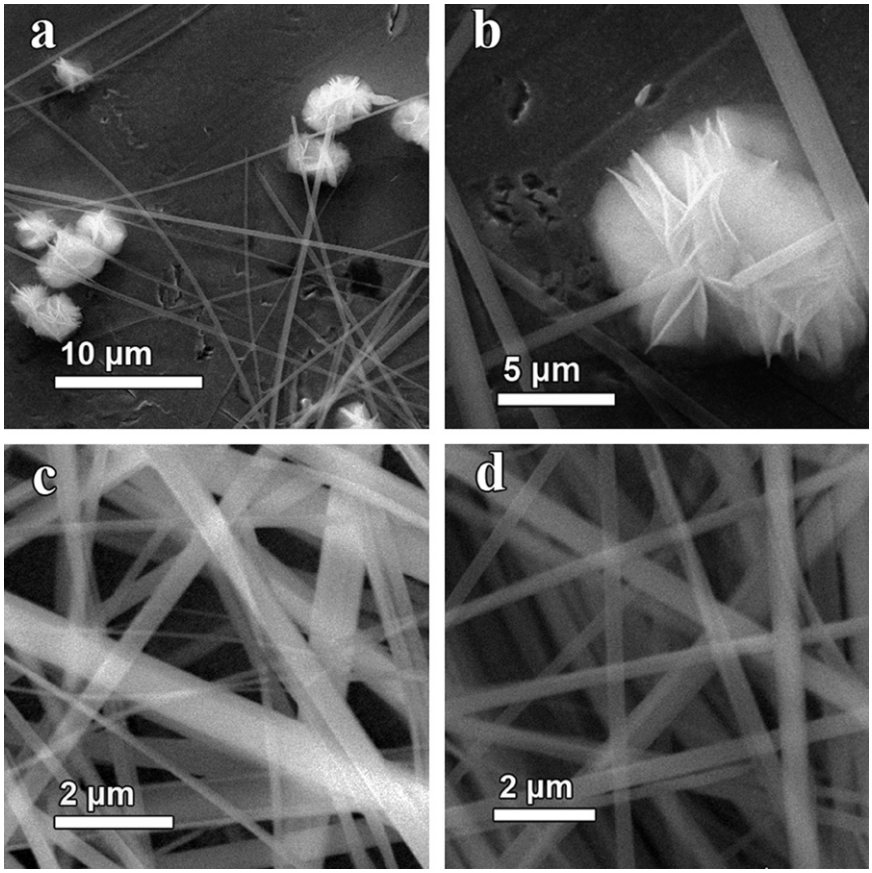

Fig. 6. SEM images of the product synthesized with only half the concentration of sodium tartrate while other conditions remained typical (a and b). SEM images of the products synthesized with different r of 1:4 (c) and 1:3 (d) while other conditions are typical.

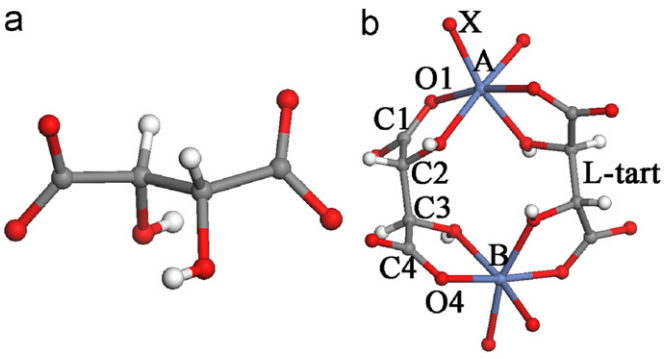

Fig. 7. Illustration of molecular structure: Tartrate (a) and the common structural building block of divalent metal tartrate salts (b).

should be further investigated in future work. Several ad hoc attempts at explaining this fail. For example, it is not so that the wires all grow in the first two hours and subsequently lose water and ethanol from their internal structure, thereby shrinking. Under this hypothesis, the mass of the sample will decrease with the reaction time, but the weight actually increases by 20% in the first four hours and then stays almost constant until $t=16$ h. A hypothesis based on a thermodynamic equilibrium being established over long times (small wires grow while large ones shrink) would be inconsistent with the observed averages and deviations on the diameters; a constant length would be very unlikely in case of such equilibration processes. Given these counter intuitive results, we would like to stress that they are reliably reproducible. For instance the 16 h samples have been prepared more than ten times.

4. Conclusions

In summary, diameter-adjustable cobalt sodium tartrate nanowires are synthesized by a simple, environmentally friendly ethanol-assisted hydrothermal route. The obtained CSTNWs have smooth surfaces and a narrow distribution in diameter. The diameters of the nanowires are time-dependent and can be controlled in a wide range of 80–250 nm by adjusting the reaction time. In the synthesis of the homogeneous CSTNWs, the optimal reaction parameters include an ethanol/water ratio of 1:2 combined with a sodium tartrate concentration of 0.225 M and a pH value above 13.5. The interactions between ligands and metal ions are responsible for the resulting amorphous metal tartrate. Ethanol and water are confirmed to participate in the formation of these nanowires via weak forces such as hydrogen and Van der Waals bonds. The anti proportional dependence between diameters and reaction time is counterintuitive but reproducible and should be investigated in further research. This will likely involve the detailed analysis of the first hour via division into yet smaller reaction times.

One-dimensional NSs usually show pronounced size effects. Combined with their extreme length and flexibility, it is reasonable to speculate that the CSTNWs will find applications as, say, thermal or electromechanical sensors. More specific suggestions must await the further study of properties. One interesting application that is currently under study is their use as precursors

for 1D porous cobalt oxides which can be employed as catalyst supports, capacitors, and as magnetic materials.

Supporting information available

HRTEM and SAED images, XRD pattern, TGA and DSC curves of the sample in the typical experiment, and TEM images of the product under pH=7.

Acknowledgments

This work was jointly supported by the PAPD, the Fundamental Research Funds for the Central Universities, the Scientific Research Foundation of Graduate School of Nanjing University, the National Natural Science Foundation of China, and the State Key Program for Basic Research of China.

Appendix A. Supplementary material

Supplementary data associated with this article can be found in the online version at doi:10.1016/j.jssc.2011.09.009.

References

[1] Oh. Moonhyun, G.B. Carpenter, D.A. Sweigart, Acc. Chem. Res. 37 (2004) 1–11.
[2] B. Moulton, M.J. Zaworotko, Chem. Rev. 101 (2001) 1629–1658.
[3] E. Suzuki, H. Kabasawa, T. Honma, R. Nozaki, Y. Shiozaki, Acta Cryst. 52 (1996) 976–981.
[4] E. Coronado, J.R. Galán-Mascarós, C.J. Gómez-García, A. Murcia-Martínez, Chem. Eur. J. 12 (2006) 3484–3492.
[5] M.G. Amiri, A. Morsali, M.Z. Zeller, Anorg. Allg. Chem. 635 (2009) 1673–1677.
[6] M. O'Keeffe, M. Eddaoudi, H. Li, T. Reineke, O.M. Yaghi, J. Solid State Chem. 152 (2000) 3–20.
[7] C. Janiak, Dalton Trans. (2003) 2781–2804.
[8] S. Kitagawa, R. Kitaura, S.L. Noro, Angew. Chem. Int. Ed. 43 (2004) 2334–2375.
[9] D. Maspoch, D. Ruiz-Molina, J. Veciana, J. Mater. Chem. 14 (2004) 2713–2723.
[10] Z. Xu, Coord. Chem. Rev. 250 (2006) 2745–2757.
[11] A.Y. Robin, K.M. Fromm, Coord. Chem. Rev. 250 (2006) 2127–2157.
[12] K. Biradha, M. Sarkar, L. Rajput, Chem. Commun. (2006) 4169–4179.
[13] K.S. Min, M.P. Suh, J. Solid State Chem. 152 (2000) 183–190.
[14] C.L. Cahill, D.T. de Lill, M. Frisch, CrystEngComm 9 (2007) 15–26.
[15] L. Carlucci, G. Ciani, D.M. Proserpio, CrystEngComm 5 (2003) 269–279.
[16] S.V.N.T. Kuchibhatla, A.S. Karakoti, D. Bera, S. Seal, Prog. Mater. Sci. 52 (2007) 699–913.
[17] N.Y. Xia, P.D. Yang, Y.G. Sun, Y.Y. Wu, B. Mayers, B. Gates, Y.D. Yin, F. Kim, H.Q. Yan, Adv. Mater. 15 (2003) 353–389.
[18] F.Y. Cui, X.Y. Ma, C. Li, T. Dong, Y.Z. Gao, Z.G. Han, Y.N. Chi, C.W. Hu, J. Solid State Chem. 183 (2010) 2925–2931.
[19] J.Y. Lu, Coord. Chem. Rev. 246 (2003) 327–347.
[20] S.C. Tang, S. Vongehr, Y. Wang, L. Chen, X.K. Meng, J. Solid State Chem. 183 (2010) 2166–2173.
[21] L.P. Zhu, W.D. Zhang, H.M. Xiao, Y. Yang, S.Y. Fu, J. Phys. Chem. C 112 (2008) 10073–10078.
[22] L.P. Zhu, H.M. Xiao, W.D. Zhang, Y. Yang, S.Y. Fu, Cryst. Growth Des. 8 (2008) 1113–1118.
[23] Y.Y. Liu, M. Grzywa, M. Weil, D. Volkmer, J. Solid State Chem. 183 (2010) 208–217.
[24] J.F. Moulder, W.F. Stickle, P.E. Sobol, K.D. Bomben, J. Chastain, Handbook of X-Ray Photoelectron Spectroscopy: A Reference Book of Standard Spectra for Identification and Interpretation of XPS Data, Perkin-Elmer Corporation, Physical Electronics Division, Minnesota, 1992.
[25] B.J. Tan, K.J. Klabunde, P.M.A. Sherwood, J. Am. Chem. Soc. 113 (1991) 855–861.
[26] Y.J. Zhang, S. Ma, D. Li, Z.H. Wang, Z.D. Zhang, Mater. Res. Bull. 43 (2008) 1957–1965.
[27] M. Bazzaoui, L. Martins, E.A. Bazzaoui, J.I. Martins, J. Electroanal. Chem. 537 (2002) 47–57.
[28] D.T. Clark, W.J. Feast, P.J. Tweedale, H.R. Thomas, J. Polym. Sci. Polym. Chem. Ed. 18 (1980) 1651–1664.
[29] R.G.J. Miller, B.C. Stace, D.M. Adams, Laboratory Methods in Infrared Spectroscopy, second ed., Heyden & Son Ltd., London, 1972.
[30] M.E. Torres, A.C. Yanes, T. Lopez, J. Stockel, J.F. Peraza, J. Cryst. Growth 156 (1995) 421–425.
[31] D. Bayot, B. Tinant, M. Devillers, Inorg. Chem. 44 (2005) 1554–1562.
[32] L.J. Bostelaar, R.A.G. de Graaff, F.B. Hulsbergen, J. Reedijk, W.M.H. Sachtler, Inorg. Chem. 23 (1984) 2294–2297.
[33] T. Gelbrich, T.L. Threlfall, S. Huth, E. Seeger, Polyhedron 25 (2006) 937–944.
[34] M. Lutz, A.M.M. Schreurs, Acta Cryst. C64 (2008) m296–m299.
[35] X.X. Zhao, J.P. Ma, Y.B. Dong, R.Q. Huang, Cryst. Growth Des. 7 (2007) 1058–1068.